Hindawi
Scientific Programming
Volume 2021, Article ID 8399153, 10 pages
https://doi.org/10.1155/2021/8399153

Research Article

Analysis of Glomerular Filtration Rate in Ischemic Cerebrovascular Diseases under the Magnetic Resonance Angiography Image Segmentation Algorithm

Yong Ding,[1] **Yuebin Liu**,[2] **Cong Peng**,[2] **Huanmei Wang**,[2] **Yuqin Xu**,[2] **Shengrong Jiao**,[2] **Huan Xu**,[3] **Yan Zhao**,[1] **and Mingyu Liu**[2]

[1]*Department of Tuina and Rehabilitation Medicine, Hubei Provincial Hospital of Traditional Chinese Medicine, Hubei Province Academy of Traditional Chinese Medicine, Hubei University of Chinese Medicine, Wuhan, Hubei 430061, China*
[2]*Department of Rehabilitation Medicine, The Ninth Hospital of Wuhan, Wuhan, Hubei 430081, China*
[3]*Coronary Care Unit, Wuhan No. 1 Hospital, Wuhan Hospital of Traditional Chinese and Western Medicine, Wuhan, Hubei 430022, China*

Correspondence should be addressed to Mingyu Liu; 1923011407@siit.edu.cn

Received 19 June 2021; Accepted 18 August 2021; Published 11 September 2021

Academic Editor: Gustavo Ramirez

In order to discuss the segmentation effect of the magnetic resonance angiography (MRA) image segmentation algorithm based on the fuzzy clustering algorithm and DR-CV model and the prognostic value of glomerular filtration rate (GFR) in the ischemic cerebrovascular disease (ICVD), a total of 178 patients who were admitted to the hospital and received MRA due to ICVD were selected as the research objects of this study. Blood vessel segmentation was performed on the MRA image by fuzzy clustering algorithm and DR-CV model, and all patients were divided into a control group (group A), a single-vessel stenosis group (group B), a two-vessel stenosis group (group C), and a multiple-vessel stenosis group (group D). The GFR was estimated by using the dietary modification equation for kidney disease, and the correlation between GFR and the severity of arterial stenosis in patients with ICVD was analyzed. It was found that the results of the Dice similarity index (DSI) of the MRA image blood vessel segmentation algorithm based on the fuzzy clustering algorithm and the integrated model of boundary and regional information (DR-CV model) were all above 85%. The age and GFR values of the four groups of patients were significantly different ($P < 0.05$). The proportions of patients in groups C and D in the group with low DFR were significantly different from those in groups A and B ($P < 0.01$); the proportions of patients in groups A and B in the high-level GFR group had extremely significant differences compared with group D ($P < 0.01$). Age, GFR, total cholesterol (TC), and high-density lipoprotein-C (HDL-C) were correlated with the degree of arterial stenosis ($P < 0.05$). It showed that the segmentation effect of MRA image blood vessel segmentation algorithm based on the fuzzy clustering algorithm and DR-CV model was better, and the GFR level can be used as an independent risk factor for the ICVD.

1. Introduction

ICVD is a common disease in clinical practice at present. The main cause of the disease is stenosis or occlusion of blood vessels in the brain, which eventually causes localized cerebral ischemic necrosis. At present, the digital subtraction angiography (DSA), electronic computed tomography angiography (CTA), and magnetic resonance angiography (MRA) are used to diagnose the ICVD patients. Among them, DSA is currently the gold standard for diagnosing the abnormal blood vessel morphology, but because of its high diagnostic cost, invasiveness, radiation exposure, and complicated and time-consuming operations, it is not suitable for initial screening and census [1]. CTA requires contrast media for imaging during the inspection process, and it has defects such as radiation and iodine contrast media allergy [2]. MRA is accepted by most doctors and patients because of its simple operation, no trauma, no

radiation, and no need for contrast agents. Clinical data shows that during the image reconstruction of MRA, part of the signal will be lost, and the small blood vessel structure and lesions cannot be fully displayed; there will also be a phenomenon of expanding the stenosis of the blood vessel; the low-velocity blood vessel is not displayed; the image of blood vessel suffers from distorted artifacts [3]. At present, the doctors are required to manually outline the contours of blood vessels in the area of interest (AOI) for image segmentation in the clinical diagnosis. This method is more time-consuming and laborious. Some researchers have proposed that the pattern recognition method, artificial intelligence method, model method, neural network method, tracking method, and other algorithms under the machine learning can be applied to the segmentation of blood vessels. Among them, the tracking method cannot perform automatic segmentation [4]; although the segmentation result of the artificial intelligence algorithm is more accurate, the algorithm is more complicated [5]; the segmentation speed of the neural network algorithm is faster, but it requires manual interaction during the calculation process [6].

GFR refers to the amount of urinary urine produced by both kidneys per unit time, and it is a heavy indicator for clinical evaluation of renal function. GFR is affected by various physiological factors such as age, diet, obesity, protein intake, and so on. Studies have found that low-level GFR is an independent risk factor for cerebrovascular events. At the same time, some studies have pointed out that the reduction of GFR has a certain correlation with the occurrence and development of cerebrovascular, and the reduction of GFR can be used as a marker of the occurrence of cardiovascular and cerebrovascular diseases [7]. However, there are few studies on the correlation between GFR and the severity of arterial stenosis in patients with ICVD.

In summary, the current MRA image segmentation technology has some shortcomings such as complex algorithms and automatic segmentation. Currently, there are few studies on MRA image segmentation. 178 patients who were admitted to our hospital and received MRA due to ICVD from January 2017 to December 2019 were selected as the research objects in this study to establish a new MRA blood vessel segmentation algorithm. It was applied in the diagnosis of patients with ICVD to further analyze the correlation between GFR and the severity of arterial stenosis in patients with ICVD. The research results of this study provided a certain reference value for the diagnosis of ICVD in the future.

2. Materials and Methods

2.1. Research Objects. 178 patients who were admitted to hospital and received MRA due to ICVD from January 2017 to December 2019 were selected as the research objects of this study, including 132 males and 46 females, with an average age of 62.58 ± 8.74 years old. The inclusion criteria were as follows: patients diagnosed with ICVD according to the diagnostic criteria established in the "Guidelines for the Diagnosis and Treatment of Acute Ischemic Stroke in China" and diagnosed with cranial DSA and MRA neuroimaging [8]. The exclusion criteria were as follows: patients with nonatherosclerotic vascular diseases such as moyamoya disease and vasculitis; patients with other neurological diseases such as intracerebral hemorrhage, brain tumors, and craniocerebral trauma; and patients with severe heart, lung, liver, kidney, and other organ dysfunctions. The experiment procedures had been approved by the Ethics Committee of the Hospital, and all the subjects included in the study had signed the informed consents.

2.2. Brainstem Segmentation Algorithm with the MRA Image. Compared with classic sets, the fuzzy set was more in line with the true thinking of human beings, so it was widely used in the field of image processing. Among the fuzzy clustering algorithms, the more mature one was the fuzzy C-mean (FCM) algorithm. The objective function of FCM was shown in equation (1), where N was the set of all pixels of the image, the total number of pixels was n; μ_{jk} was the membership of the jth pixel belonging to the kth group, and the $\sum_{k=1}^{C} \mu_{jk} = 1$ was satisfied. x_j was the gray value of the jth pixel, and v_k was the center gray of the kth group. C was the number of grouping categories, and m was the weighted index of membership.

$$J = \sum_{j \in N} \sum_{k=1}^{C} {\mu_{jk}}^{m} \left\| x_j - v_k \right\|^2. \tag{1}$$

The derivatives of J to μ_{jk} and v_k were taken to obtain the minimum value of J, and it was inserted into $\sum_{k=1}^{C} \mu_{jk} = 1$; then calculate the membership degree μ_{jk} and the center gray v_k of the j^{th} pixel in the k^{th} group.

$$\mu_{jk} = \left[1 + \sum_{j=1}^{C} \left(\frac{\left\| x_k - v_i \right\|^2}{\left\| x_k - v_j \right\|^2} \right)^{1/m-1} \right], \tag{2}$$

$$v_k = \frac{\sum_{k=1}^{n} \left(\mu_{jk} \right)^m \cdot x_k}{\sum_{k=1}^{n} \left(\mu_{jk} \right)^m}. \tag{3}$$

In equations (2) and (3), x_k was the gray value of the kth pixel; $\|x_k - v_i\|$ was the modulus of the inner product; C was the number of grouping categories; and m was the weighted index of membership.

The brainstem segmentation method mainly was composed by four steps: image preprocessing, extraction of initial brainstem edge texture, small block boundary segmentation and merging in target area, and two texture segmentations. The specific segmentation process was as follows: after performing gray-scale clustering on the MRA image to be segmented, the seed point of the image was determined to obtain the initial binary cut picture, the white picture of the brainstem edge texture was extracted to find out the target area around the brainstem, then the small block boundaries of the target area were segmented, and the segmented areas were merged. After two texture segmentations and reverse processing of the picture, the brainstem segmentation image was finally obtained, as shown in Figure 1.

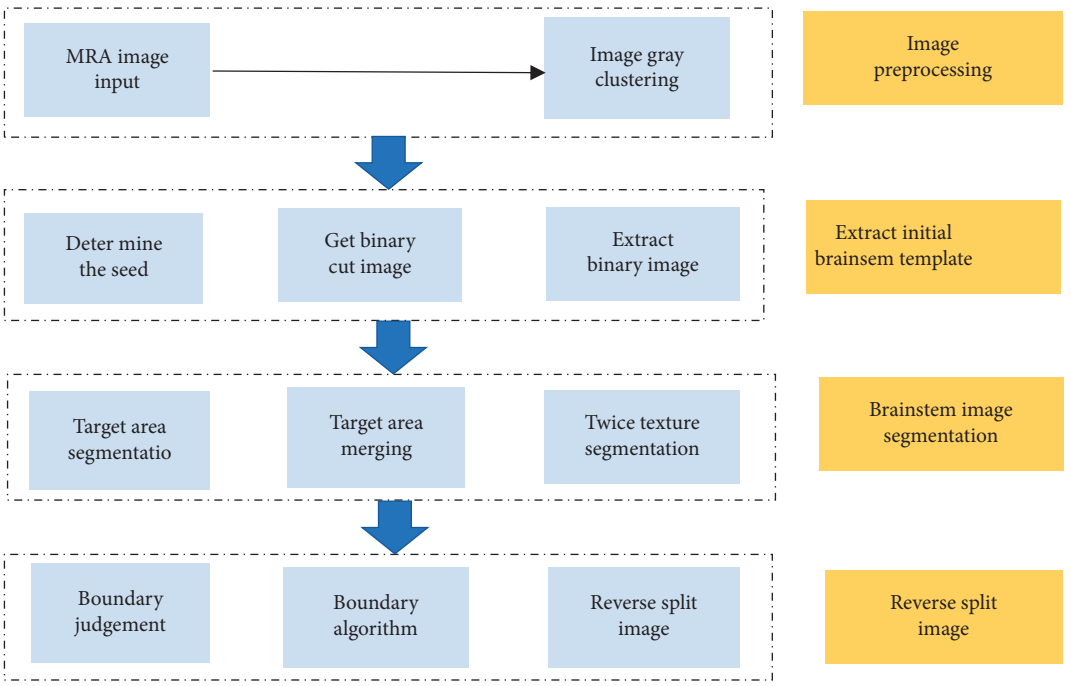

Figure 1: Flowchart of brainstem segmentation algorithm with the MRA image.

2.3. Blood Vessel Segmentation Algorithm with the MRA Image. The segmentation algorithm based on the deformation model provided a new solution for correctly segmenting regions with irregular boundaries in the image. The active contour of the parametric active contour model was energetic. The image segmentation process was the process of the curve always moving, and finally the weighted value of minimal value of both the internal energy and the external energy of the model were reached. The active contour curve was expressed as

$$X(s,t) = [x(s,t), y(s,t)]. \tag{4}$$

In equation (4), X was the two-dimensional coordinate point, t was the time parameter, and s was the normalized arc length parameter; thus, $s \in [0,1]$. When the active contour model image moved in the spatial region, its energy function can be expressed as

$$E(X) = E_{\text{in}}(X) + E_{\text{ex}}(X). \tag{5}$$

In equation (5), $E_{\text{in}}(X)$ was the internal energy to drive the expansion and contraction of the contour curve.

Then, the following equation can be obtained:

$$E_{\text{in}}(X) = \frac{1}{2}\int_0^1 \left[\alpha(s)\left|\frac{\partial X}{\partial s}\right|^2 + \beta(s)\left|\frac{\partial^2 X}{\partial s^2}\right|^2\right] \mathrm{d}s. \tag{6}$$

$E_{\text{ex}}(X)$ was the external energy, giving the motion direction of the parameter active contour; thus, $E_{\text{ex}}(X) = -|\nabla G_\sigma A I(x,y)|^2$; α was the elastic coefficient; β was the rigidity coefficient; ∇ was the gradient operator; σ represented the standard deviation of the Gaussian function $G_\sigma(x,y)$; and A represented the curl operator.

The energy function was minimized with the variational principle; then, the active contour curve could meet the following equation:

$$\frac{\partial}{\partial s}\left(\alpha\frac{\partial X}{\partial s}\right) - \frac{\partial}{\partial s^2}\left(\beta\frac{\partial^2 X}{\partial s^2}\right) - \Delta E_{\text{ex}} = 0. \tag{7}$$

If it was expressed by internal force and external force, it can be expressed as $F_{\text{in}}(X) + F_{\text{ex}}(X) = 0$; the internal force can be given as follows:

$$F_{\text{in}}(X) = \frac{\partial}{\partial s}\left(\alpha\frac{\partial X}{\partial s}\right) - \frac{\partial}{\partial s^2}\left(\beta\frac{\partial^2 X}{\partial s^2}\right). \tag{8}$$

And the external force can be $F_{\text{ex}}(X) = -\Delta E_{\text{ex}}$; in equation (8), α was the elastic coefficient; β was the rigidity coefficient; ∇ was the gradient operator; and s indicated the normalized arc length parameter. The algorithm of DR-CV model was built based on the deformation model, and the total energy function can be expressed as follows:

$$E(\varphi) = E_{\text{in}}(\varphi) + E_{\text{ed}}(\varphi) + E_{\text{re}}(\varphi), \tag{9}$$

where $E(\varphi)$ was the total energy of the DR-CV model; $E_{\text{in}}(\varphi)$ represented the internal energy of the DR-CV model; $E_{\text{ed}}(\varphi)$ represented the external edge energy of the DR-CV model; and $E_{\text{re}}(\varphi)$ referred to the external area energy of the DR-CV model. For the image $I(x,y)$, the calculation method of gradient descent flow in the DR-CV model was as shown in the following equation:

$$\begin{aligned}\frac{\partial\varphi}{\partial t} = -\frac{\partial E}{\partial\varphi} &= d_p(|\nabla\varphi|)\nabla\varphi + a\delta(\varphi)\left[g(\nabla I)\frac{\nabla\varphi}{|\varphi|}\right] \\ &+ (1-\beta)\delta(\varphi)\left[(I(x,y)-c_1)^2 - (I(x,y)-c_2)^2\right],\end{aligned} \tag{10}$$

where c_1 was the average internal gray value of evolution curve of the DR-CV model; c_2 was the average external gray value of evolution curve of the DR-CV model; and $g(\nabla I)$ referred to the boundary indicator function, which can be calculated by the following equation:

$$g(\nabla I) = \frac{1}{1 + \left|\nabla G_\sigma AI\right|}, \tag{11}$$

where ∇ was the gradient operator and ∇I was the gradient of the image.

The specific algorithm flow of segmenting the MRA image by using the fuzzy clustering algorithm were as follows: the MRA image was input and preprocessed, and the brainstem portion in the MRA image was extracted to obtain the brainstem image expansion. The MRA image was segmented primarily by using the difference and binarization to obtain the ideal brainstem area. Finally, the intracranial blood vessels were segmented secondarily based on the related algorithms of the MRA image blood vessel segmentation in the DR-CV model to obtain the blood vessel segmentation image (Figure 2).

2.4. Evaluation Methods of MRA Image Segmentation. Evaluation methods of MRA image segmentation generally included the experimental method and analytical method. The experimental method was used to verify in this study. The specific process of experimental verification is shown in Figure 3. The golden standard image was obtained by manual labeling method, and the success index μ and DSI of quantitative index segmentation were used to evaluate the results of MRA image segmentation. The success factor of segmentation can be expressed as $\mu = S_1/S_2 \times 100\%$, of which S_1 represented the total number of pixels correctly segmented in the MRA image; S_2 represented the total number of pixels in the segmentation result of the MRA image.

The DSI expression equation can be written as follows:

$$D(M, N) = 2 \times \frac{|M \cap N|}{(|M| + |N|)} \times 100\%, \tag{12}$$

where M represented the gold standard image; N referred to the segmented MRA image to be evaluated; $M \cap N$ was the surface value of the overlapping area of the two MRA images; $|M|$ indicated the area of the gold standard image; and $|N|$ was the area of the segmented MRA image to be evaluated. If DSI > 0.7, it indicated that the consistency between the result and the gold standard was high, and the segmentation effect was good.

2.5. Calculating Method and Grouping of GFR. The GFR was estimated according to the dietary improvement equation for kidney disease, and the specific GFR calculation method was shown as follows:

$$\begin{aligned} \mathrm{GFR} = {} & 170 \times (\mathrm{Scr})^{-0.99} \times (\mathrm{Age})^{-0.176} \times (\mathrm{BUN})^{-0.170} \\ & \times (\mathrm{Alb})^{0.318}, \end{aligned} \tag{13}$$

where Scr referred to the serum creatinine; Age referred to the patient's age; BUN represented the blood urea nitrogen; and Alb was the albumin. All patients were divided into a low-level group (GFR < 83.93, 59 cases), a middle-level group (83.93 < GFR < 101.42, 60 cases), and a high-level group (GFR > 101.42, 59 cases) based on the GFR classification criteria [9].

2.6. Cerebral Angiography Methods and Grouping. Before the surgery, blood routine, urine routine, liver function, computed tomography (CT), and MRI as well as other routine examinations were performed; fasting and water were not allowed for 12 hours before the surgery. The patients were operated on with the routine disinfection on the puncture sites, anesthetized with local infiltration anesthesia, punctured with the femoral artery with a modified Seldinger technique, inserted with an arterial sheath, and the aortic arch angiography was performed to observe the general direction of the blood vessels above the aortic arch, abnormal blood vessels, and advantages of the cone situation. After the surgery, a saline bag was used to compress the puncture site for 6–8 hours to prevent bleeding, and it should be observed whether the patient's lower extremity was swollen. The cerebral angiography images of all patients were assessed by an experienced physician. The angiography results were judged separately by three physicians. The patients were divided into four groups based on the number of diseased vessels and stenosis rate (>50%): group A was the control group (46 cases), group B was the single-vessel stenosis group (44 cases), and group C was the two-vessel stenosis group (41 cases), and group D was the multiple-vessel stenosis group (47 cases).

2.7. Statistical Methods. The SPSS21.0 statistical software was used to analyze the data. The measurement data of normal distribution was expressed as mean ± standard deviation ($\overline{x} \pm s$), t-test was used for intergroup comparison based on two independent samples, chi-square test was used for counting data, Pearson's correlation analysis was used to analyze the correlation between the GFR and the severity of arterial stenosis in patients with ICVD, and $P < 0.05$ was considered as the difference that had a statistical significance.

3. Results

3.1. MRA Image Segmentation Results. The MRA image of the target area marked by the doctor was obtained and taken as the gold standard of the doctor's manual standard, as shown in Figure 4. The segmented MRA image was obtained after segmentation. In this study, the MRA image was segmented based on the DR-CV model to obtain the brainstem segmented image. The boundary was extracted from the primarily segmented MRA image through the DR-CV model. Due to the small blood vessel area, the active contour was shrunk inward to a certain extent to get the best boundary extraction effect picture. The template of the secondary segmentation image was obtained on the basis of the extracted image of the boundary, and then the secondary segmentation result of the MRA image was obtained with the

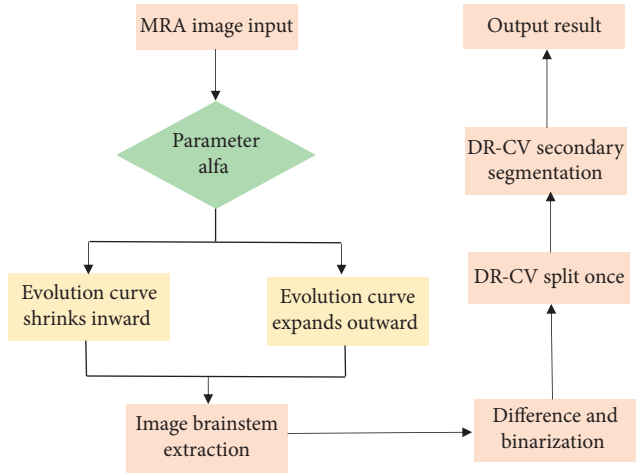

Figure 2: Flowchart of intracranial blood vessel segmentation algorithm based on the DR-CV model.

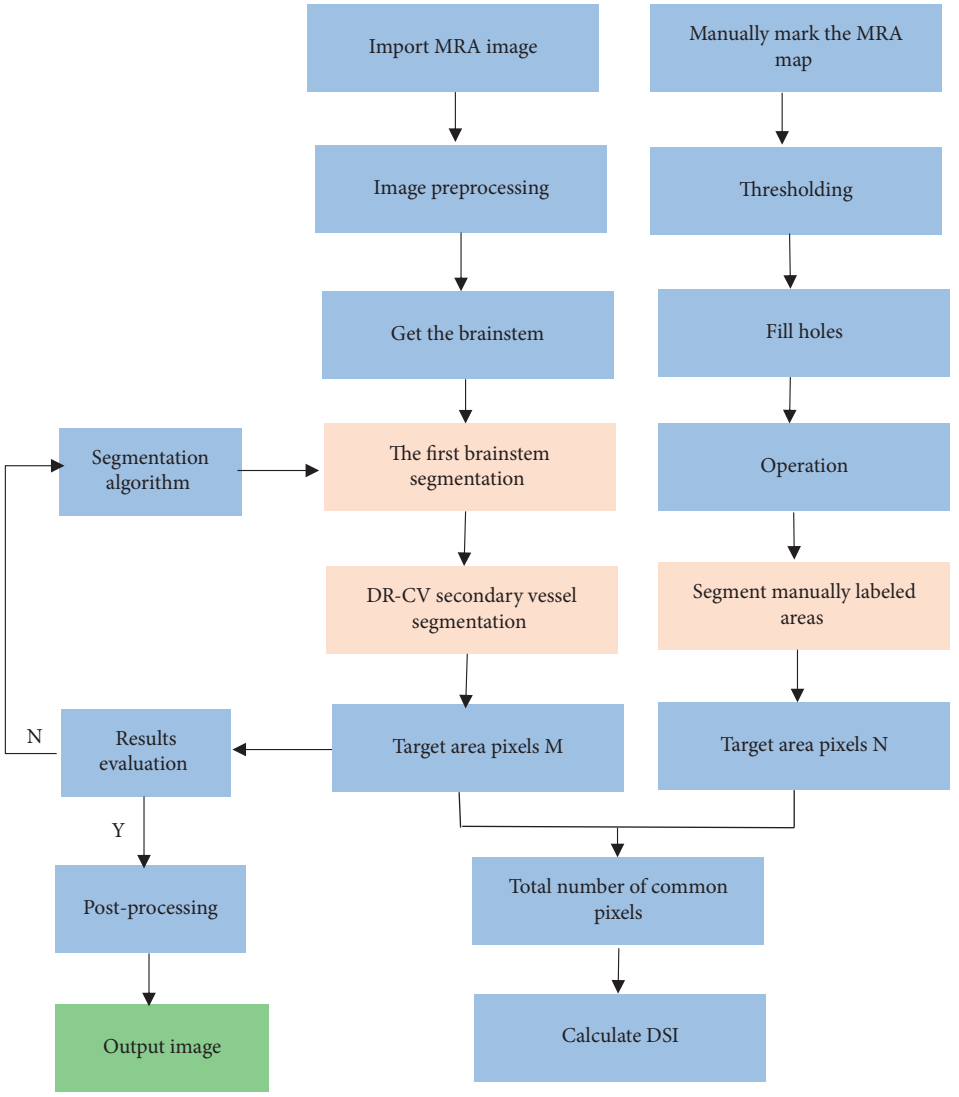

Figure 3: Flowchart of evaluation on MRA image segmentation.

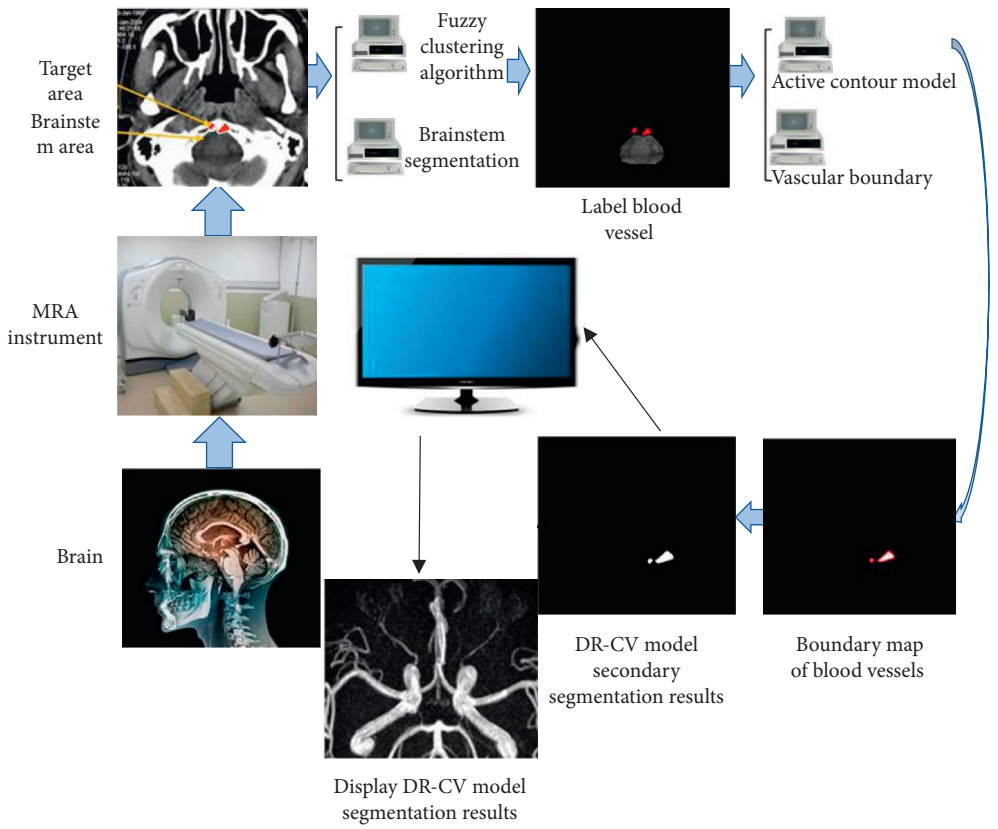

Figure 4: Flowcharts and images for blood vessel segmentation of the MRA image based on DR-CV.

template of the secondary segmentation image. After magnifying it, it was the final blood vessel segmentation result.

3.2. Evaluation of MRA Image Segmentation. The MRA image was obtained based on the blood vessel segmentation algorithm of the DR-CV model, and the comparison and analysis on the segmentation similarity coefficient DSI between the obtained MRA image and the blood vessel segmentation image of gold standard were taken. The obtained DSI results are shown in Figure 5. It can be known from Figure 5 that the MRA image blood vessel segmentation results of 178 patients were compared with the blood vessel segmentation results of gold standard. The DSI of blood vessel segmentation results of the MRA images for 178 patients with ICVD reached more than 85%, and the DSI for most of the blood vessel segmentation results of the MRA image was above 95%.

3.3. Comparison of Basic Data of Patients in Four Groups. The basic data of patients in the four groups were compared, and the results are shown in Table 1. It can be seen from Table 1 that there was no significant difference among the basic data of the four groups of patients such as gender, history of hypertension, and history of diabetes. The difference was not statistical significance ($P > 0.05$). The age increased with the increase of the number of vascular lesions, and there was a significant difference ($P < 0.05$).

3.4. Comparison of Biochemical Indexes of Patients in Four Groups. The statistical analysis on TC, TG, HDL-C, LDL-C, VLDL-C, and BUN for patients in four groups was performed, and the results are given in Figure 6(a). It can be seen from Figure 6 that the TC value of patients in groups B, C, and D was higher than that in group A ($P < 0.05$), and the HDL-C value of patients in groups B, C, and D was lower than that in group A ($P < 0.05$). There was no significant difference for biochemical indexes TG, LDL-C, VLDL-C, and BUN for the four groups of patients ($P > 0.05$). The comparison of Scr and UA for patients in four groups had no obvious difference ($P > 0.05$), as shown in Figure 6(b). The HB, Alb, and GFR for patients in four groups were compared and analyzed, and the results are shown in Figure 6(c). It can be found that there was no obvious difference for HB and Alb for patients in four groups ($P > 0.05$); the GFR value of patients in groups B, C, and D was lower than that in group A, and the differences were significant ($P < 0.05$); the GFR value of patients in groups C and D had obvious difference with that in group B ($P < 0.05$), and the GFR value of patients in groups C and D had no significant difference ($P < 0.05$).

3.5. Comparison of Severity of Arterial Stenosis in Patients with Different Levels of GFR. The severity of arterial stenosis was compared and analyzed in three patients with different levels

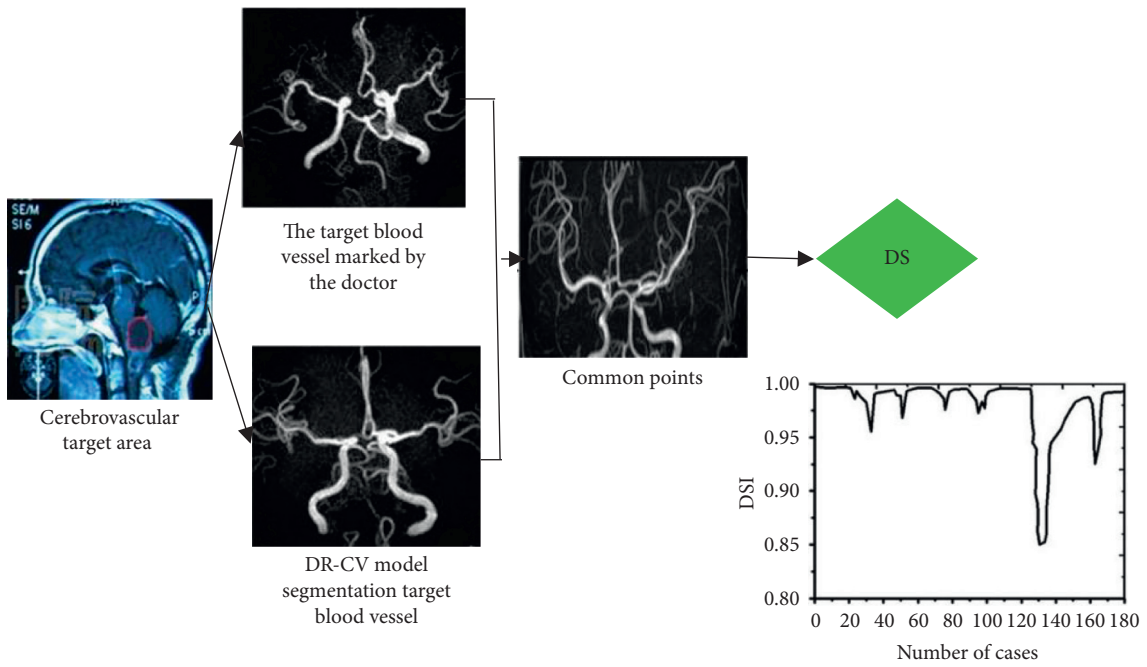

Figure 5: DSIs of the blood vessel for the patient with ICVD and the gold standard.

Table 1: Comparison of basic data of patients in four groups.

Group	Group A	Group B	Group C	Group D	P value
Male (patients (%))	30 (65.22)	31 (75.61)	35 (79.55)	31 (65.95)	0.421
Age (years)	60.19 ± 9.82	61.57 ± 8.82	64.05 ± 9.25	67.53 ± 10.24	0.043
Height (cm)	165.42 ± 9.93	167.26 ± 10.15	166.82 ± 10.29	166.75 ± 11.03	0.327
Weight (kg)	61.19 ± 4.82	59.91 ± 3.39	60.07 ± 5.03	58.97 ± 2.94	0.258
BMI (kg/m^2)	23.52 ± 0.98	20.31 ± 0.83	24.03 ± 0.72	22.75 ± 0.63	0.226
History of diabetes	7 (15.22)	8 (19.51)	7 (15.91)	10 (21.28)	0.151
History of hypertension	22 (47.83)	21 (51.22)	19 (43.18)	24 (51.06)	0.107

of GFR, and the results are shown in Figure 7. From Figure 7, it can be seen that the percentages of patients in groups C and D with low GFR were higher, which were 27.12% and 44.07%, respectively, and they were extremely significantly different compared with those in group A and group B ($P < 0.01$); there was no significant difference between the proportions of patients in groups A, B, C, and D in the middle-level group ($P > 0.05$); the proportions of patients in group A and group B in the high-level group were higher, which were 38.98% and 35.59%, respectively; the proportions of patients in groups A and B were significantly different from those in group D ($P < 0.01$); the proportion of patients in group C in the high-level group was 22.03%, which was significantly higher than that in group D of 8.47%, so the difference was obvious ($P < 0.05$).

3.6. Multifactor Analysis of Arterial Stenosis in Patients with ICVD. The age, gender, body mass index (BMI), diabetes, hypertension, GFR, TC, LDL-C, HDL-C, VLDL-C, HB, Scr, BUN, UA, and Alb were taken as independent variables, and the presence or absence of arterial stenosis was taken as the dependent variable for the single-factor logistic regression analysis. The results are shown in Table 2. From Table 2, it can be seen that the four factors of age, GFR, TC, and HDL-C were correlated with the degree of arterial stenosis ($P < 0.05$), which can be used as the risk factors for arterial stenosis in patients with ICVD.

4. Discussion

The fuzzy clustering algorithm was used to perform the edge feature processing and brainstem segmentation extraction in the brainstem regions with classification significance based on the characteristics of the brainstem itself on the MRA image in this study. Then, the regions near the brainstem were selected and analyzed, and the vessel segmentation of the MRA image was performed based on the blood vessel segmentation algorithm of the DR-CV model. The MRA images obtained by the segmentation algorithm were compared and analyzed with the blood vessel images marked by the professional doctors. The results revealed that the DSI of the MRA image segmentation using the blood vessel segmentation algorithm reached more than 85%, and the DSI of the blood vessel segmentation results of the most MRA images was more than 95%. Bibiloni et al. [10] used the

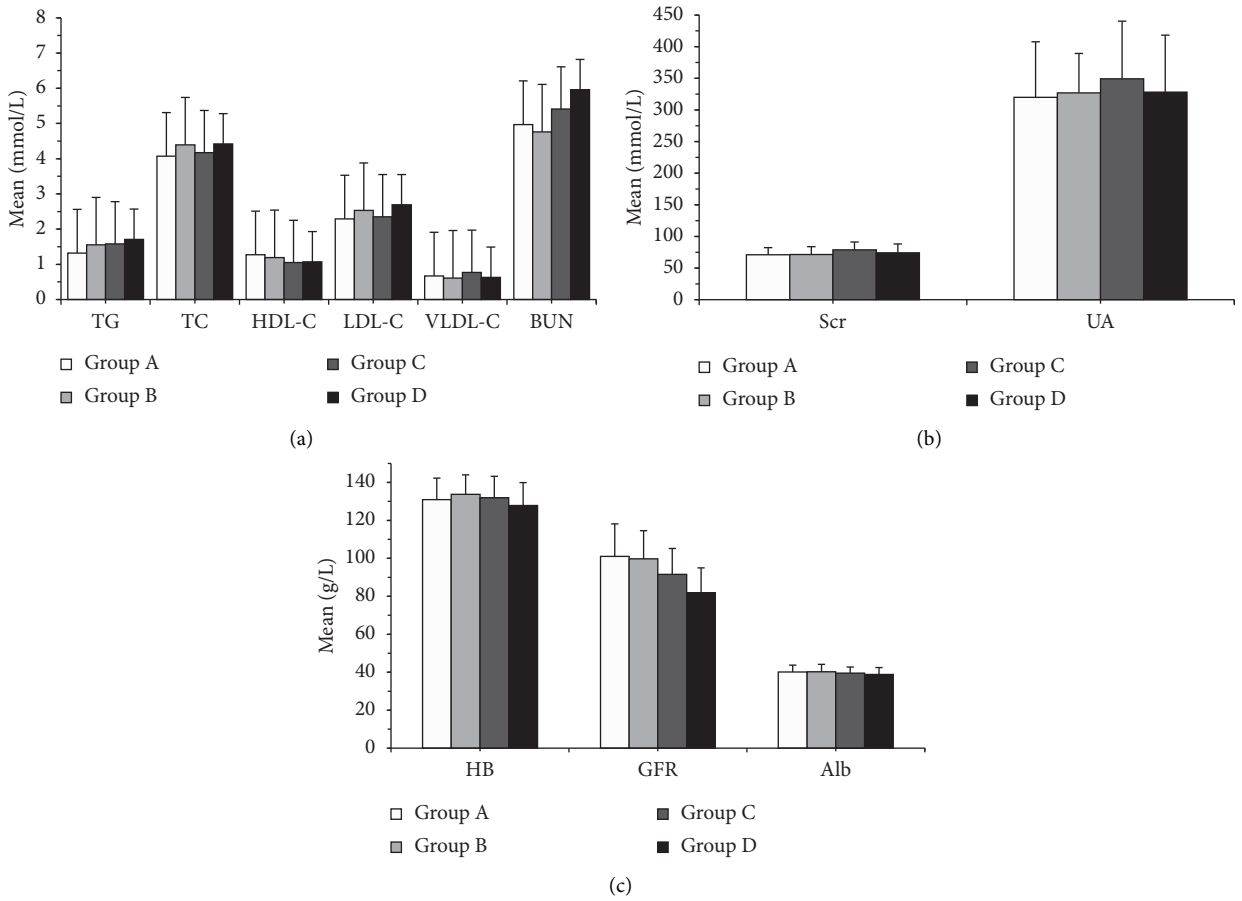

Figure 6: Comparison of biochemical indexes of patients in four groups. (a) The comparison of TC, TG, HDL-C, LDL-C, VLDL-C, and BUN of patients in four groups. (b) The comparison of Scr and UA of patients in four groups. (c) The comparison on HB, Alb, and GFR for patients in four groups (*indicated that the difference was obvious by comparing with group A, $P < 0.05$).

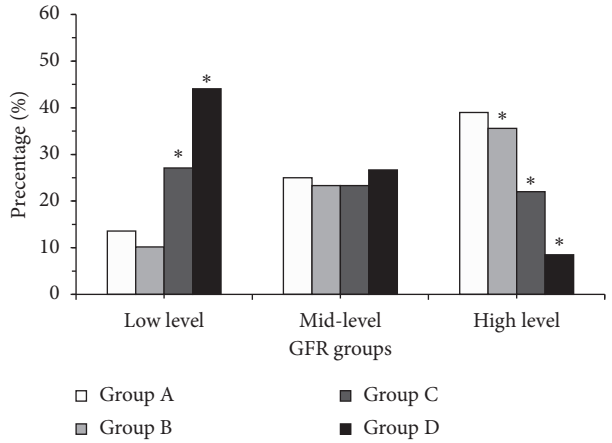

Figure 7: Comparison of severity of arterial stenosis in patients with different levels of GFR (*indicated that the difference was obvious by comparing with group A, $P < 0.05$).

fuzzy clustering algorithm to separate the blood vessels of the X-ray image and found that the blood vessel separation image obtained by the fuzzy clustering algorithm was better. At the same time, some researchers [11] found that the similarity index of the image obtained after segmentation and the image marked by the doctor reached more than 80% if using an improved active contour model to segment the MRI image blood vessels, and the segmentation result was good. In this study, the algorithm was further optimized on the basis of the contour model, and the DR-CV model was

Table 2: Logistic regression analysis of risk factors for arterial stenosis in patients with ICVD.

Factor	Regression coefficient	Standard error	Wald $\chi 2$ value	Risk ratio	95% CI	P value
Age	0.051	0.021	5.365	1.082	1.005–1.067	0.025
Gender	0.434	0.427	0.551	1.863	0.512–3.518	0.429
BMI	0.717	0.325	2.336	2.644	0.835–5.126	0.081
Diabetes	0.723	0.495	3.141	2.118	0.837–5.277	0.096
Hypertension	0.885	0.357	4.497	2.094	0.828–5.764	0.457
GFR	−0.015	0.076	4.368	1.008	0.981–0.933	0.032
TC	0.515	0.276	5.368	1.708	1.181–2.933	0.012
LDL-C	0.693	0.424	3.675	1.724	0.842–5.723	0.476
HDL-C	−1.325	0.553	3.861	0.363	0.126–0.947	0.035
VLDL-C	0.829	0.435	4.417	1.809	0.862–4.526	0.512
HB	0.275	0.262	0.863	1.335	0.786–2.581	0.344
Scr	0.325	0.356	1.012	1.253	0.672–2.783	0.401
BUN	0.157	0.085	2.123	1.195	0.327–0.746	0.187
UA	0.253	1.928	1.769	1.083	0.718–2.939	0.523
Alb	0.419	0.525	0.613	1.526	0.552–3.574	0.517

obtained. The similarity index of the image segmented based on this model to the active contour model is significantly higher than the research results of Bibiloni et al. (2019), indicating that the blood vessel segmentation algorithm based on the DR-CV model had high consistency with the blood vessel segmentation results of the MRA image, so the segmentation results were valid.

At present, the detection of GFR is realized by some indirect methods, which are generally estimated by the renal clearance or plasma clearance of biomarkers. The commonly used methods include inulin clearance, radionuclide labeling, serum creatine estimation method, and estimation with kidney disease diet improvement equation. Among them, the inulin clearance is used to estimate the GFR, but it is currently clinically used less frequently due to its cumbersome measurement process and higher testing costs [12]. The detection process of the radionuclide labeling is radioactive with relatively high price, and it cannot be used by special groups such as pregnant women, infants, and young children [13]. The estimation of GFR by serum creatine estimation method is susceptible to the use of meat by the examinee and the vigorous exercise before the detection, so the results are biased [14]. In summary, after analyzing the pros and cons of various GFR estimation methods, the estimation method of kidney disease diet improvement equation was used to estimate the GFR of patients with ICVD. A large number of research results indicated that the accuracy of GFR detection by modification of diet in renal disease (MDRD) is higher than that of serum creatine estimation method and Coekcroft-Gault formula [15].

A large number of studies have shown that the reduction of GFI is an independent risk factor for cardiovascular and cerebrovascular diseases. Some researchers [16] found that the risk of ischemic stroke increased by 43% in patients with $\mathrm{GFR} < 60\mathrm{Ml}/(\mathrm{min} * 1.73\,\mathrm{m}^2)$, indicating that GFR reduction is a risk factor for ischemic and hemorrhagic cerebrovascular disease. This is consistent with the results of this study. After a single-factor logistic regression analysis of related factors, it was found that GFR was a risk factor for arterial stenosis in patients with ICVD. The possible reason was that when the GFR changes, it could cause changes in the patient's pathophysiological conditions such as oxidative stress response, inflammatory response, abnormal calcium, and phosphorus metabolism, which in turn caused the risk of cardiovascular and cerebrovascular diseases [17]. At the same time, the results of this study also found that age, TC, and HDL-C were also risk factors for ICVD. Under the normal physiological conditions, HDL-C combined with polyanionic mucopolysaccharide was deposited on the structural membrane of the glomerular basement membrane. When a pathological condition occurred, the thickness of the lipid on the glomerular basement membrane increased significantly, which in turn caused the blood lipids and lipoprotein metabolism, and which thus caused cardiocerebrovascular disease and increased the prevalence and mortality of the ICVD.

5. Conclusion

In this study, a blood vessel segmentation algorithm was established for MRA images based on the fuzzy clustering algorithm and DR-CV model, and on this basis, the correlation between the GFR and ischemic cerebrovascular disease was studied and analyzed. The results revealed that the segmentation algorithm of blood vessel segmentation algorithm of MRA images based on the fuzzy clustering algorithm and DR-CV model was better. There was a significant correlation between the level of GFR and the degree of arterial stenosis in patients with ICVD, which can be used as an independent risk factor for the ICVD. However, there were still some deficiencies in this article. This study was a retrospective analysis, with a small number of collected cases, so it was limited due to some reasons. It had to increase the amount of sample collections in the later coworking and validate the postoperative value of GFI in the ICVD. In summary, it established the blood vessel segmentation algorithm of MRA image based on the fuzzy clustering algorithm and DR-CV model in this study. On this basis, it was found that the level of GFR was an independent risk factor of the ICVD, which provided a certain reference value for clinical diagnosis of ICVD in the future.

Data Availability

The data used to support the findings of this study are available from the corresponding author upon request.

Conflicts of Interest

The authors declare no conflicts of interest.

Authors' Contributions

Yong Ding and Yuebin Liu contributed equally to this work.

References

[1] G. Bruce and B. Erskine, "Analysis of time delay between computed tomography and digital subtraction angiography on the technical success of interventional embolisation for treatment of lower gastrointestinal bleeding," *Journal of medical radiation sciences*, vol. 67, no. 1, pp. 64–71, 2020.

[2] J. Kwiecinski, D. Dey, S. Cadet et al., "Predictors of 18F-sodium fluoride uptake in patients with stable coronary artery disease and adverse plaque features on computed tomography angiography," *European Heart Journal - Cardiovascular Imaging*, vol. 21, no. 1, pp. 58–66, 2020.

[3] B. J. Carroll, M. L. Schermerhorn, W. J. Manning et al., "Imaging for acute aortic syndromes," *Heart*, vol. 106, no. 3, pp. 182–189, 2020.

[4] X. Y. Zhou, Z. W. Tay, P. Chandrasekharan et al., "Magnetic particle imaging for radiation-free, sensitive and high-contrast vascular imaging and cell tracking," *Current Opinion in Chemical Biology*, vol. 45, pp. 131–138, 2018.

[5] S. Moccia, E. De Momi, S. El Hadji, and L. S. Mattos, "Blood vessel segmentation algorithms - review of methods, datasets and evaluation metrics," *Computer Methods and Programs in Biomedicine*, vol. 158, pp. 71–91, 2018.

[6] A. Oliveira, S. Pereira, C. A. Silva et al., "Retinal vessel segmentation based on fully convolutional neural networks," *Expert Systems with Applications*, vol. 112, pp. 229–242, 2018.

[7] A. Wilhelm-Bals, C. Combescure, H. Chehade, Y. Daali, and P. Parvex, "Variables of interest to predict glomerular filtration rate in preterm newborns in the first days of life," *Pediatric Nephrology*, vol. 35, no. 4, pp. 703–712, 2020.

[8] Y. Fan, X. Liao, Y. Pan, K. Dong, Y. Wang, and Y. Wang, "Intravenous thrombolysis is safe and effective for the cryptogenic stroke in China: data from the thrombolysis implementation and monitor of acute ischemic stroke in China (TIMS-China)," *Journal of Stroke and Cerebrovascular Diseases*, vol. 28, no. 1, pp. 220–226, 2019.

[9] H. Liu, H. Zheng, P. Wu et al., "Estimated glomerular filtration rate, anemia and outcomes in patients with ischemic stroke," *Annals of Translational Medicine*, vol. 8, no. 1, p. 2, 2020.

[10] P. Bibiloni, M. González-Hidalgo, S. Massanet et al., "A real-time fuzzy morphological algorithm for retinal vessel segmentation," *Journal of real-time image processing*, vol. 16, no. 6, pp. 2337–2350, 2019.

[11] M. Chung, J. Lee, J. W. Chung, and Y.-G. Shin, "Accurate liver vessel segmentation via active contour model with dense vessel candidates," *Computer Methods and Programs in Biomedicine*, vol. 166, pp. 61–75, 2018.

[12] F. Leion, J. Hegbrant, E. Den Bakker et al., "Estimating glomerular filtration rate (GFR) in children. The average between a cystatin C- and a creatinine-based equation improves estimation of GFR in both children and adults and enables diagnosing Shrunken Pore Syndrome," *Scandinavian Journal of Clinical and Laboratory Investigation*, vol. 77, no. 5, pp. 338–344, 2017.

[13] W.-T. K. Tsai and A. M. Wu, "Aligning physics and physiology: engineering antibodies for radionuclide delivery," *Journal of Labelled Compounds and Radiopharmaceuticals*, vol. 61, no. 9, pp. 693–714, 2018.

[14] J. P. Law, S. Di Gerlando, T. Pankhurst, and L. Kamesh, "Elevation of serum creatinine in a renal transplant patient following oral creatine supplementation," *Clinical Kidney Journal*, vol. 12, no. 4, pp. 600-601, 2019.

[15] H. S. Kilbride, P. E. Stevens, G. Eaglestone et al., "Accuracy of the MDRD (modification of diet in renal disease) study and CKD-EPI (CKD epidemiology collaboration) equations for estimation of GFR in the elderly," *American Journal of Kidney Diseases*, vol. 61, no. 1, pp. 57–66, 2013.

[16] B. Thomas, K. Matsushita, K. H. Abate et al., "Global cardiovascular and renal outcomes of reduced GFR," *Journal of the American Society of Nephrology*, vol. 28, no. 7, pp. 2167–2179, 2017.

[17] M. F. Blum, A. Surapaneni, J. D. Stewart et al., "Particulate matter and albuminuria, glomerular filtration rate, and incident CKD," *Clinical Journal of the American Society of Nephrology*, vol. 15, no. 3, pp. 311–319, 2020.